

Finite element simulations on the mechanical properties of MHS materials

Z. Y. Gao · T. X. Yu · D. Karagiozova

Received: 10 May 2006 / Accepted: 4 September 2006 / Published online: 10 January 2007
© Springer-Verlag 2007

Abstract Finite element simulations are carried out to examine the mechanical behavior of the metallic hollow sphere (MHS) material during their large plastic deformation and to estimate the energy absorbing capacity of these materials under uniaxial compression. A simplified model is proposed from experimental observations to describe the connection between the neighboring spheres, which greatly improves the computation efficiency. The effects of the governing physical and geometrical parameters are evaluated; whilst a special attention is paid to the plateau stress, which is directly related to the energy absorbing capacity. Finally, the empirical functions of the relative material density are proposed for the elastic modulus, yield strength and plateau stress for FCC packing arrangement of hollow spheres, showing a good agreement with the experimental results obtained in our previous study.

Keywords Cellular material · Hollow sphere · Large plastic deformation · Numerical simulation · FEM

The project supported by the Hong Kong Research Grant Council (RGC) (HKUST 6079/00E) and the National Natural Science Foundation of China (10532020).

Z. Y. Gao · T. X. Yu (✉) · D. Karagiozova
Department of Mechanical Engineering,
Hong Kong University of Science & Technology,
Clear Water Bay, Kowloon, Hong Kong, China
e-mail: metxyu@ust.hk

D. Karagiozova
Institute of Mechanics, Bulgarian Academy of Sciences,
Acad. G. Bonchev Street, Block 4, Sofia 1113, Bulgaria

1 Introduction

Cellular materials such as honeycombs and foams are widely applied in cushioning, packaging and other impact/shock protecting owing to their excellent energy-absorbing capacity with a long plateau range and a controllable plateau stress. However, traditional cellular solids, especially closed-cell metallic foams, have large varieties in the size, shape and distribution of cells as produced in the manufacturing process, which make their stress–strain relation highly unrepeatable. Consequently, it is difficult to precisely monitor their mechanical properties.

Now the development of the metallurgy allows the production of single hollow sphere with highly controlled characteristics (e.g., diameter and wall thickness) from lots of base materials, and those hollow spheres can be bonded by epoxy resin, soldered and sintered to form new types of cellular materials. A detailed review on the manufacturing process was made by Waag et al. [1]. Compared with conventional foams, these materials have much better geometric uniformity and fewer defects, resulting in good mechanical and acoustic properties. Among them, the sintered metallic hollow sphere (MHS) materials are most suitable for energy absorption because of the high strength and ductility of both the bonding and base materials.

The hollow sphere foams first attracted attentions in 1990s, when lots of metallurgists began to develop new types of cellular materials in view of the drawbacks of the traditional foams. The early studies were focused on the fabrication. On the basis of an experimental study of MHS specimens made of stainless steel, Lim et al. [2] found that their quasi-static behavior is quite close to that of the open cell foams. Adopting the concept of



Fig. 1 Samples of the cellular materials composed of metallic hollow spheres and bonded by sintering technique (MHS)

regular stacking of atoms, Sanders et al. [3,4] defined some elementary parameters (such as bonding angle, relative sphere wall thickness h/R) and proposed fairly good finite element models for those with regular stacking patterns. Meanwhile, similar finite element models were also proposed by Gasser et al. [5–7]. However, all these studies were restricted to the elastic response and the initial yielding behavior, probably because of the dramatic increase of the computational time in the simulation of the large plastic deformations of their models.

Systematic experimental and analytical studies were also reported on two types of MHS specimens made of mild steel in previous papers [8–10], where the deformation process, the quasi-static behavior and the dynamic response were described in detail. Observation of the cross-section of the MHS sample shows that simplified finite element models can be adopted to improve the computation efficiency. By simulating the large plastic deformation of the MHS material, the present paper is aimed to further understand the large deformation mechanisms and the effects of the parameters which govern the mechanical behaviors.

2 Experimental results of two types of MHS materials

Comprehensive experimental studies [8] were carried out to examine the mechanical properties of two types of MHS specimens with relative densities less than 6% shown in Fig. 1. The radii of the two types of spheres were $R_L = (1.50 \pm 0.13)$ mm (large spheres) and $R_S = (0.90 \pm 0.13)$ mm (small spheres), with the thicknesses of $h_L = (0.049 \pm 0.013)$ mm and $h_S = (0.049 \pm 0.011)$ mm, respectively. The relative densities of the MHS materials were $\rho_L^*/\rho_0 = 0.052 \pm 0.002$ and $\rho_S^*/\rho_0 = 0.045 \pm 0.002$, respectively, provided that the density of the base material (mild steel) is $\rho_0 = 7,800$ kg/m³. The bonding angle θ , referring to a half of the connecting neck, was obtained as $\theta_L \in (5^\circ, 20^\circ)$ and $\theta_S \in (5^\circ, 30^\circ)$, respectively.

The quasi-static uniaxial compression tests were performed on a universal testing machine MTS 810 with

a load cell of 50 kN and a loading speed of 1 mm/min. The MHS specimens were cut from the original material plate in the form of a cuboid (36 mm × 36 mm × 25 mm) or a cylinder ($\phi 25$ mm × 25 mm). A fairly good repetition of the stress–strain curves was achieved and a typical nominal stress–strain curve for a specimen made of the MHS material with smaller spheres is plotted in Fig. 2a. The stress–strain curve can be divided into three distinct phases: the elastic phase, the “plateau” phase and the densification phase, while the average “plateau” stress is defined as:

$$\sigma_{pl}^* = \frac{\int_{\varepsilon_Y}^{\varepsilon_D} \sigma^*(\varepsilon) d\varepsilon}{\varepsilon_D - \varepsilon_Y}, \quad (1a)$$

where ε_Y and ε_D correspond to the yield strength and the strain at densification; ε_D is defined as the strain value corresponding to the stationary point in the “efficiency” versus strain curve where the “efficiency” renders a global maximum, i.e., $[d\eta(\varepsilon)/d\varepsilon]_{\varepsilon=\varepsilon_D} = 0$, as shown by the dashed line in Fig. 2a, where the “efficiency” is defined by

$$\eta(\varepsilon_a) \equiv \frac{\int_0^{\varepsilon_a} \sigma^*(\varepsilon) d\varepsilon}{\sigma^*(\varepsilon_a)} \quad (1b)$$

High speed dynamic tests were performed with a modified SHPB testing system, in which nylon bars were chosen to increase the impedance ratio [8]. Significant enhancements were observed for both the initial crushing stress and the average plateau stress (up to an 86% enhancement compared to the quasi-static plateau stress), see Fig. 2b. Corresponding enhancing mechanisms are identified, where the micro-inertia effect accounts for the appearance of the sharp initial peak, whilst the strain-rate sensitivity of the base material (mild steel) accounts for the significant enhancement for the plateau stress.

3 Finite element models

3.1 Simplification of the connection between neighboring spheres

Since the MHS materials adopted in our study were fabricated by a sintering process whilst a minor pre-compression was applied, the randomly packed hollow spheres were connected in small flattened contact regions instead of points. Figure 3a shows a typical cross-section of the specimen where the flattened regions can be clearly seen among the neighboring spheres. A simplified model of the connection based on this

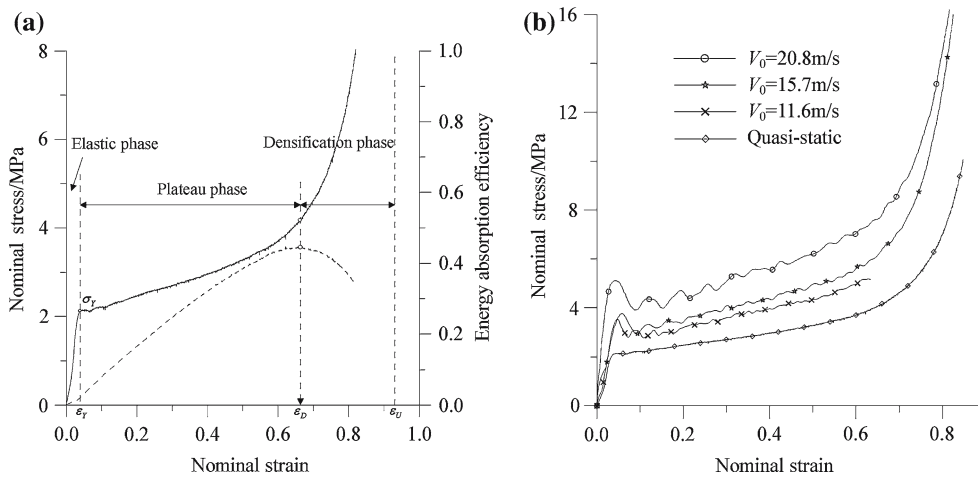


Fig. 2 Typical stress–strain curve of MHS material with small spheres. **a** Static loading and the energy absorption efficiency; **b** Dynamic loading

observation is constructed as shown in Fig. 3b. The connection region is a circular plate with radius of $r = R \cdot \sin \theta$ and thickness of $2h$. The main advantage of this model is that it can be simulated with finite-strain S3R shell elements in order to significantly reduce the computation time; whereas the limitation is that the bonding angle can not be very large in order to satisfy the geometric similarity with the hollow spheres. In the present study, the bonding angle is restricted to a range of 0° – 15° .

3.2 Description of the representative blocks

Although the commercial finite element software serves as a powerful tool in solving engineering problems, it is greatly restricted by the computational ability of the computers available. The computation time will be extremely long if too many nodes and elements are adopted in a model. Therefore, it is not feasible to simulate the whole structure of a specimen used in the experiment. The basic unit of the MHS material is a hollow sphere with uniform outer radius, hence it is straightforward to adopt the concept of regular packing of atoms in crystal solids when constructing the finite element models. Although the hollow spheres in a real specimen are randomly packed, the specimen’s behavior can be related to a structure with regular packing, provided the relative density of the real material is appropriately taken into account in interpreting the computational results.

As well known, there exist four types of regular packing in crystal solids: the simple cubic packing (SC), the body-centered cubic packing (BCC), the face-centered cubic packing (FCC) and the hexagonal close

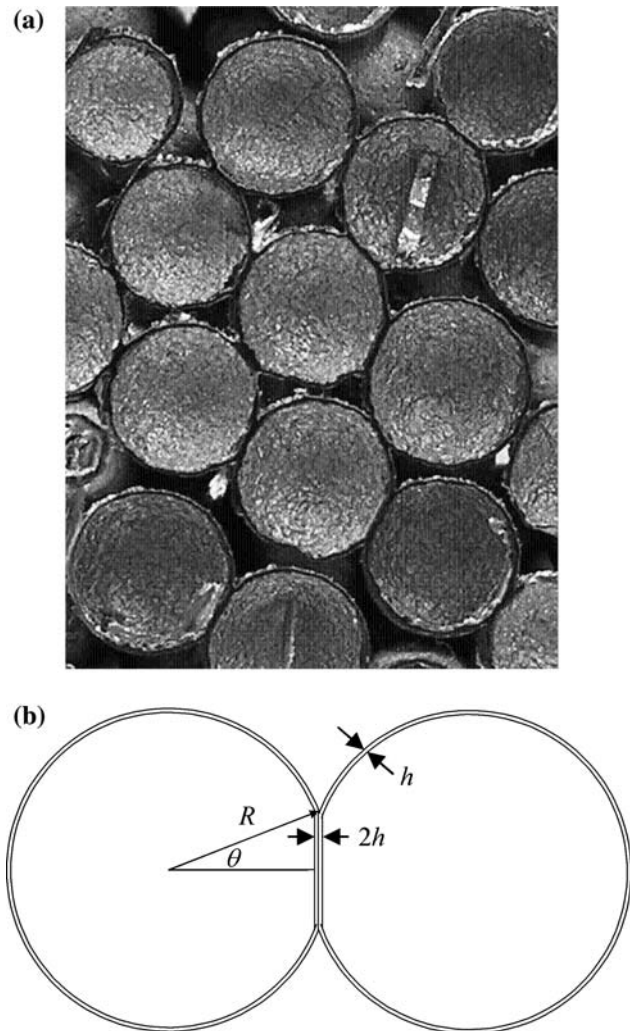
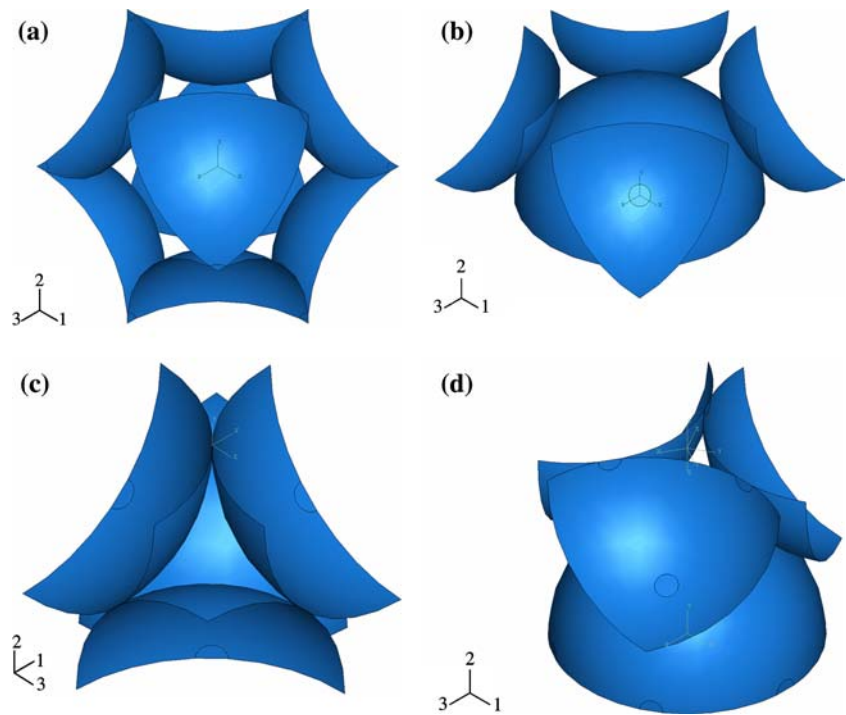


Fig. 3 **a** Typical cross-section of the MHS specimen; **b** Simplification of the connection in the present study

Fig. 4 **a** Representative block of the SC packing; **b** Representative block of the BCC packing; **c** Representative block of the FCC packing; **d** Representative block of the HCP packing



packing (HCP). By applying the appropriate boundary conditions, one can choose a small representative block to study the properties of the whole structure, see Fig. 4a–d.

3.3 Construction of the finite element models

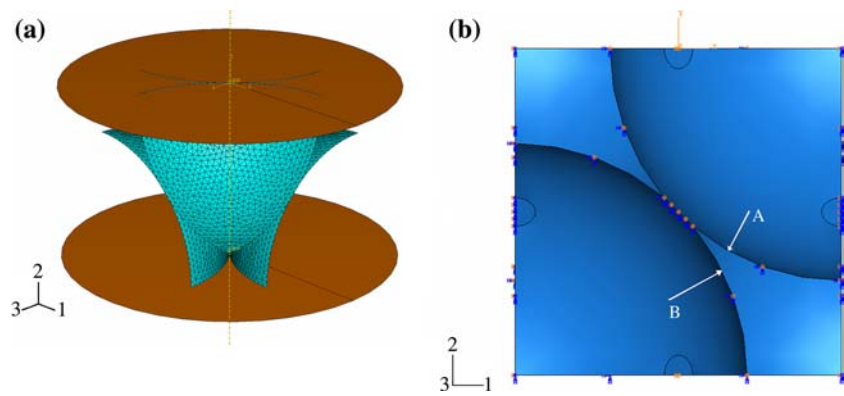
Finite element models of four types of regular packing are created by using commercial code ABAQUS v.6.4. The models are designed to evaluate the effects of the governing physical and geometrical parameters on the mechanical response, especially the crushing behavior, of different packing patterns. As shown in Fig. 5a, the deformable representative block is placed between two rigid circular plates. The bottom one serves as the fixed boundary whereas the top one serves as the punch, so that only the displacement in the vertical direction (the axis 2) is allowed. The side faces of the block are perpendicular to the axis 1 and the axis 3 except those in the HCP packing, whose cross-section in the 1–3 plane is a hexagon; while the compression is performed along the vertical direction. The “hard contact” algorithm in ABAQUS is adopted to describe the normal properties of all the contacts (i.e., the contacts between the rigid plates and the spherical shells as well as the contacts between the spherical shell parts themselves), whereas the tangential behavior is defined as frictionless. Periodic boundary conditions are not easy to be applied by using the available code for the representative blocks with complex geometries, so that symmetric boundary

conditions are used for all the vertical side faces. For example, the plane containing edge A and edge B (i.e. the plane containing the axes 1 and 2) in Fig. 5b is a symmetric plane perpendicular to the axis 3, hence the displacements along the axis 3 and the rotation angles about the axes 1 and 2 are constrained for all the nodes at these two edges. By applying the symmetric boundary conditions, the transverse expansion (or shrink) of the representative block is fully constrained. This is different from the real experiments, where the side faces remain as free boundaries. Finally, the representative block is automatically meshed by using the triangular S3R shell elements, and about 5,400–6,800 nodes are used in one hollow sphere after a mesh convergence analysis.

3.4 Geometry variation

A parametric study is performed to evaluate the effect of the relative density on the behavior of MHS material. It is known that the three important parameters are the relative sphere wall thickness, the bonding angle and the packing pattern. FCC packing is chosen as an example to study the effects of the first two parameters. According to the experimental data, the sphere wall thickness is taken to be 0.049 mm. For a given bonding angle of 5° , h/R varies from 0.01 to 0.1; for a given relative sphere wall thickness of 0.033 (i.e., for the large sphere specimen with $R = 1.5$ mm and $h = 0.05$ mm used in our experiments [8]), θ varies from 0° to 15° ; for the comparison among different packing patterns, these

Fig. 5 **a** Construction of the finite element model; **b** Corresponding boundary conditions



two parameters are set to be $h/R = 0.033$ and $\theta = 5^\circ$. Detailed geometrical parameters adopted in each case are listed in Table 1.

3.5 Material definition

Besides the relative density, a parametric study is also performed to examine the effect of the base material properties. For most of the models, the material is defined to be elastic, perfectly-plastic, with the Young's modulus varying from 50 GPa to 400 GPa and the yield stress varying from 100 to 400 MPa. As mentioned in our previous paper [8], 344 MPa is used as the yield stress of the base material (mild steel) when comparing the finite element simulation with the experimental data. Finally, the Poisson's ratio is taken as 0.3 for all the cases.

4 Results and discussions

In total more than 80 cases are programmed into ABAQUS v.6.4 and processed on personal computers (PIII 1 GHz, 1 G Ram). The non-linear geometric analysis is enabled in ABAQUS because the compressed representative block would undergo large deformations. A static approach (ABAQUS Standard) is used to obtain the elastic response and the initial yielding property, whereas a dynamic approach (ABAQUS Explicit) with an extremely large mass and a low speed is applied to achieve a large strain plastic deformation. A convergence study shows that an element length equal to 5% of the sphere radius is sufficient. For consistency, the nominal engineering strain is defined as the displacement of the top rigid plate divided by the initial height of the block, and the nominal stress is defined as the reaction force (in the static approach) or the inertia force ($-M_{\text{plate}} \cdot a$ in the dynamic approach) of the top rigid plate divided by the cross-sectional area of the block. After the FE computation, the stress-strain curves are

smoothed by a moving average method to reduce the disturbance of the contact noise.

4.1 Deformation process

As an example, the simulated deformation of the FCC packing are plotted at different stages of compression in Fig. 6. The color contours show the equivalent plastic strain at integration points, where the blue regions undergo elastic deformation and the red regions yield the largest plastic deformation. As the top rigid plate goes down, four basic parts of the FCC packing deform simultaneously. The plastic regions first occur at the four side connections and then develop with the contact regions among different parts. The strain field within the representative block is highly non-uniform, where the plastic deformation merely concentrates on the contact regions while most of the other regions experience elastic deformation only. It is also noted that there is no plastic deformation at the top (or bottom) corners in each basic part (such as region A or region B in Fig. 6) before the densification, so those regions move as rigid shell segments, which form a basic assumption adopted in our theoretical modeling [10].

4.2 Construction of the entire stress-strain curves

In the static approach, the Riks method in ABAQUS is used to simulate the early response of the representative block. The advantage of this method is that its computation efficiency is high whilst a displacement control is implemented, so the reaction force of the top rigid plate is equal to the total force acting on the block. However, the automatic computing displacement step, especially in large strains, will become so small that the simulation will halt. An equivalent dynamic approach is adopted via the ABAQUS Explicit in order to obtain the plastic behavior in large strains. The inertia effect caused by the dynamic loading is minimized by using a very low

Table 1 Geometric properties of various packing patterns

Model	h/R	$\theta(^{\circ})$	Relative density, ρ^*
FCC	0.033 (large sphere)	0	0.0703
		5	0.0710
		10	0.0734
		15	0.0771
		0.054 (small sphere)	0.1158
HCP	0.01	5	0.0222
		0.1	0.2030
BCC	0.033	5	0.0710
SC			0.0653
Sphere wall thickness			0.0502
		$h = 0.049$ mm	

loading speed, and an extremely large mass is assigned to the top rigid plate to keep the loading speed almost constant. Although there is no convergence problem in the explicit approach, the contact noise at the very beginning is so large that the early response is not reliable. The entire stress–strain curves are constructed by the combination of the two approaches, as shown in Fig. 7, where the curves coincide in the intersection region. In the subsequent analysis, the results from the Riks method are used as the early response ($\varepsilon \leq 10\%$), and the results from the explicit method are used as the later response ($\varepsilon > 10\%$).

4.3 Effects of the parameters of the base material

The FCC model with $h/R = 0.033$ and $\theta = 5^{\circ}$ is chosen to evaluate the effects of the parameters of the base material.

4.3.1 Young's modulus

The Young's modulus E of the base material is varied in the region 50–400 GPa to study its effect, whilst the yield stress is fixed as $Y = 200$ MPa. The results are listed in Table 2 and plotted in Fig. 8. On one hand, the elastic modulus of the representative block is proportional to that of the base material; on the other hand, the output parameters listed in Table 2 are quite close to each other, indicating that the Young's modulus has little effect on the MHS' plastic behavior in large strains.

4.3.2 Yield stress

The yield stress Y of the base material is varied in the region 100–400 MPa to study its effect, whilst the Young's modulus is fixed as $E = 200$ GPa. The results are listed in Table 3 and plotted in Fig. 9a and b. It is noted that the elastic modulus of the representative

Table 2 Effect of the Young's modulus of the base material

E (GPa)	E^* (GPa)	ε_D (%)	σ_{pl}^* (MPa)
50	0.54	67.7	3.76
100	1.07	67.9	3.78
200	2.15	67.9	3.78
400	4.30	67.8	3.79

FCC packing with $h/R = 0.033$ and $\theta = 5^{\circ}$, $Y = 200$ MPa

Table 3 Effect of the yield stress of the base material

Y (MPa)	E^* (GPa)	σ_Y^* (MPa)	ε_Y (%)	ε_D (%)	σ_{pl}^* (MPa)
100	2.15	1.50	0.13	66.0	1.96
200	2.15	2.97	0.26	67.9	3.78
400	2.15	5.72	0.44	68.5	7.29

FCC packing with $h/R = 0.033$ and $\theta = 5^{\circ}$, $E = 200$ GPa

block is not affected by the yield stress, whereas both the initial yield stress and the plateau stress of the representative block are proportional to the yield stress of the base material (Fig. 9a). The shapes of the stress–strain curves are similar to each other except the magnitudes of the stresses (Fig. 9b). All the above results are consistent with the plastic theory of thin-walled structures, where Y plays a dominant role in the plastic behavior.

4.3.3 Strain-rate sensitivity

Significant enhancements of the stress–strain curves were observed in dynamic tests compared with that of the quasi-static tests (Fig. 2b). A rough theoretical analysis shows that the strain-rate sensitivity of the base material is the key factor. In the finite element simulations, the Cowper–Symonds relationship [11] is adopted, where the material constants are taken as $D = 40 \text{ s}^{-1}$ and $q = 5$ for mild steel, and the results are plotted in Fig. 10. For a loading speed of 20 m/s, the plateau stress shows a 67% enhancement, comparable to 76%

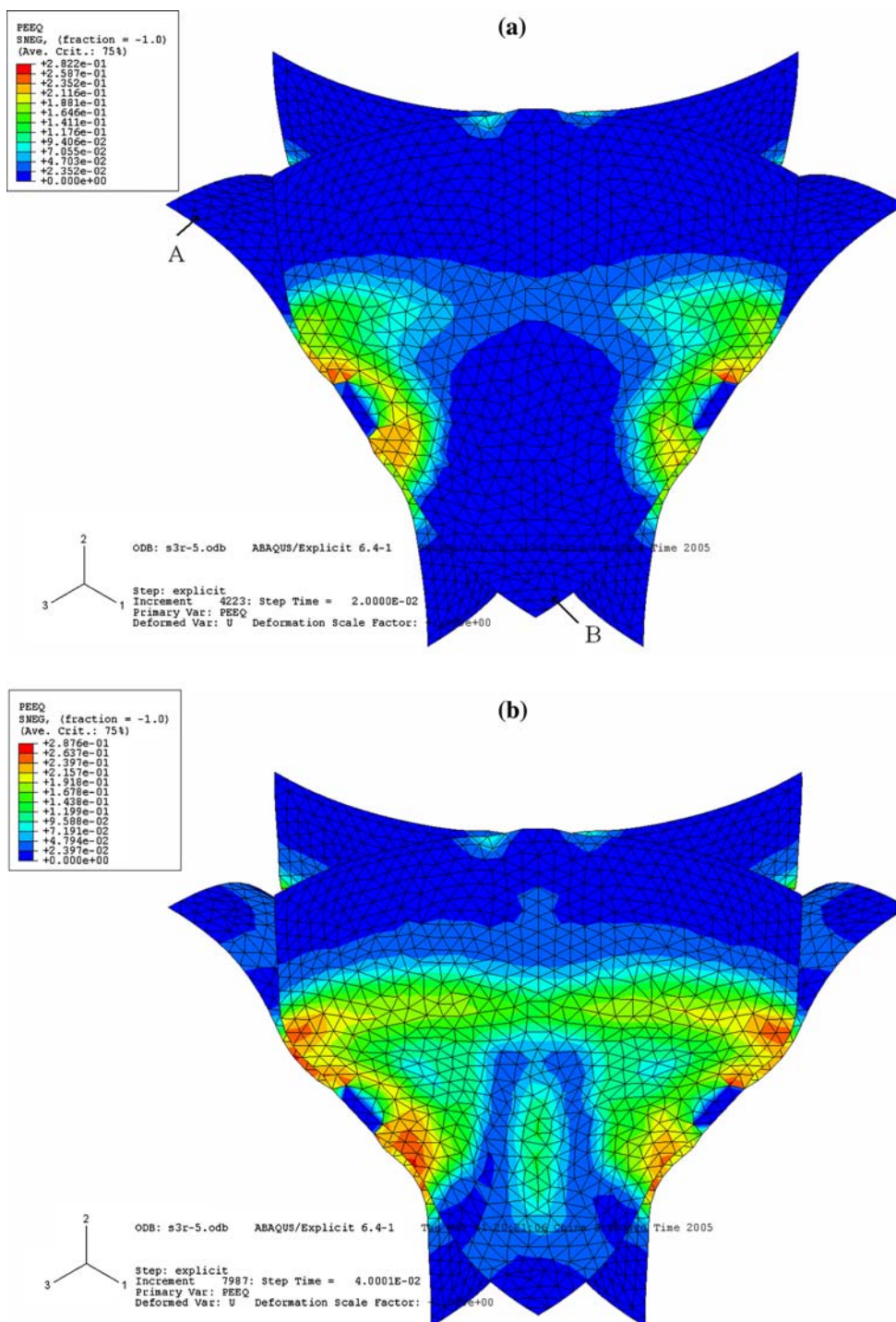


Fig. 6 Deformation of the FCC packing at different stages. **a** $\epsilon = 9.5\%$; **b** $\epsilon = 18.9\%$

in the experiment. Although a certain difference exists between these two values, the finite element simulation does demonstrate that the strain-rate sensitivity of the base material is responsible for the significant enhancement of the dynamic stress–strain curves of the MHS material.

4.4 Effects of the geometrical parameters

An elastic, perfectly-plastic relationship with $E = 200\text{GPa}$ and $Y = 200\text{MPa}$ is chosen to represent the base material when evaluating the effects of the geometrical parameters.

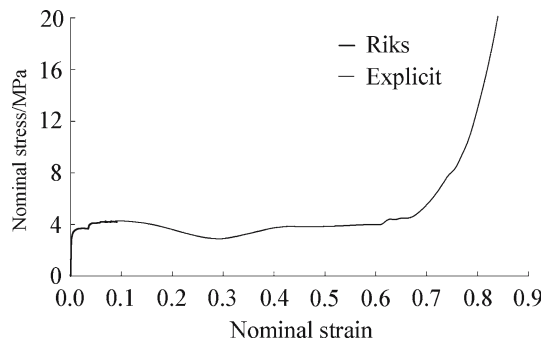


Fig. 7 Construction of an entire stress–strain curve

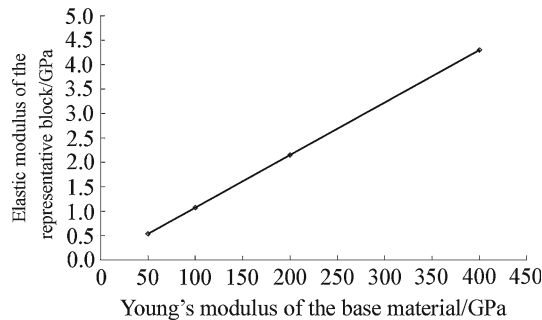


Fig. 8 Effect of the Young's modulus of the base material; FCC packing with $h/R = 0.033$ and $\theta = 5^\circ$, $Y = 200$ MPa

4.4.1 Bonding angle

The FCC model with $h/R = 0.033$ is employed in the study of the effect of the bonding angle θ , which varies from 0° to 15° . The results are listed in Table 4 and plotted in Fig. 11a and b. In the early response, both the elastic modulus and the initial yield stress of the representative block increase with the increasing bonding angle (Fig. 11a). This agrees well with the experimental observation on ping pang balls [13]. In the later response, the model with $\theta = 5^\circ$ yields the lowest plateau stress and the model with $\theta = 15^\circ$ produces the highest one among the simulated cases. In fact, it is known from Table 1 that the relative density in the case of $\theta = 5^\circ$ is larger than that in the case of $\theta = 0^\circ$. However, the latter has a larger plateau stress, indicating that besides the relative density, the internal structure (e.g., the bonding between spheres) also affects the plastic behavior. It is not sufficient to study foam materials only from the material point of view, a structural approach is also indispensable.

4.4.2 Relative sphere wall thickness

The FCC model with $\theta = 5^\circ$ is employed in the study of the effect of the relative sphere wall thickness h/R , which varies from 0.01 to 0.1. The results are listed in

Table 4 Effect of the bonding angle

$\theta/(^\circ)$	E^* (GPa)	σ_Y^* (MPa)	$\varepsilon_Y/(\%)$	$\varepsilon_D/(\%)$	$\sigma_{pl}^*/(\text{MPa})$
0	1.72	1.48	0.11	69.4	4.0
5	2.15	2.97	0.26	67.9	3.78
10	2.73	4.35	0.29	67.9	4.18
15	3.32	4.85	0.23	66.9	4.66

FCC packing with $h/R = 0.033$; $E = 200$ GPa, $Y = 200$ MPa

Table 5 Effect of the relative sphere wall thickness

h/R	E_{FCC}^* (GPa)	σ_Y^* (MPa)	$\varepsilon_Y/(\%)$	$\varepsilon_D/(\%)$	σ_{pl}^* (MPa)
0.01	0.59	0.69	0.18	71.5	0.64
0.033	2.15	2.97	0.26	67.9	3.78
0.054	3.87	5.58	0.29	67.2	8.59
0.1	8.03	12.3	0.36	72.1	22.2

FCC packing with $\theta = 5^\circ$; $E = 200$ GPa, $Y = 200$ MPa

Table 5 and plotted in Fig. 12a and b. The elastic modulus, the initial yield stress and the plateau stress all increase with the increasing relative sphere wall thickness. This is because both the stiffness and the deformation energy of the sphere increase with the increase of h/R . By a numerical fitting of the finite element results, the above three parameters are well described by the following empirical functions:

$$\frac{E^*}{E} = 0.53 \left(\frac{h}{R} \right)^{1.13}, \quad (2a)$$

$$\frac{\sigma_Y^*}{Y} = 1.08 \left(\frac{h}{R} \right)^{1.25}, \quad (2b)$$

$$\frac{\sigma_{pl}^*}{Y} = 3.82 \left(\frac{h}{R} \right)^{1.54}, \quad (2c)$$

for an FCC packing with $0.01 \leq h/R \leq 0.1$ and $\theta = 5^\circ$. In Eqs. (2a)–(2c), E^* , σ_Y^* and σ_{pl}^* denote the Young's modulus, the initial yield stress and the plateau stress of the FCC packed MHS material, respectively.

Equation (2a) is plotted in Fig. 13a. It is seen that the variation of the elastic modulus is comparable to the corresponding predictions given in Ref.[7]. Equations (2b) and (2c) are plotted in Fig. 13b. It is seen that the yield strength and the plateau stress resemble the tendency given by the experimental results. The present finite element approach for the stress–strain response of MHS material gives a reliable estimate for the material strength in relatively large strains.

4.4.3 Packing pattern

In the study of the effect of the packing pattern, the two governing geometric parameters are fixed as

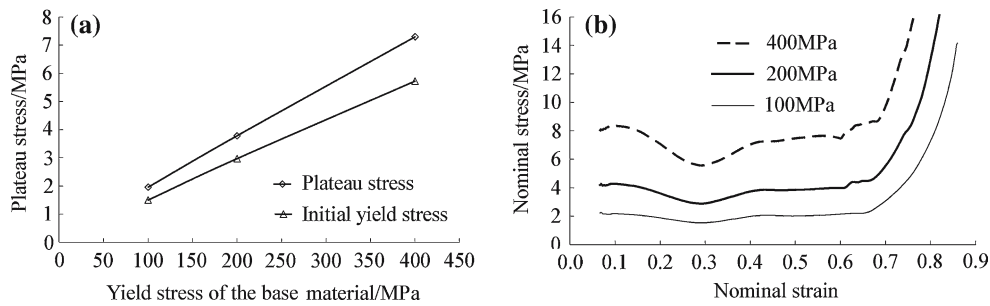


Fig. 9 Effect of the yield stress of the base material; FCC packing with $h/R = 0.033$ and $\theta = 5^\circ$, $E_{\text{raw}} = 200$ GPa: **a** The initial yield and plateau stresses; **b** Stress–strain curves

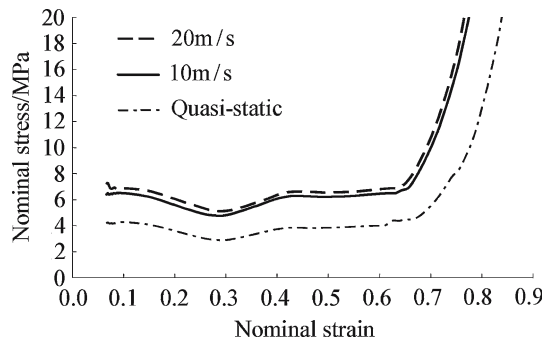


Fig. 10 Effect of the strain-rate sensitivity of the base material; FCC packing with $h/R = 0.033$ and $\theta = 5^\circ$; $E = 200$ GPa, $Y = 200$ MPa

Table 6 Effect of the packing pattern

Packing pattern	E^* (GPa)	σ_Y^* (MPa)	$\varepsilon_Y/(\%)$	$\varepsilon_D/(\%)$	σ_{pl}^* (MPa)
SC	0.25	0.36	0.28	69.2	2.41
BCC	1.74	2.39	0.23	71.3	3.12
FCC	2.15	2.97	0.26	67.9	3.78
HCP	1.74	2.20	0.21	66.3	4.05

$h/R = 0.033$, $\theta = 5^\circ$; $E = 200$ GPa, $Y = 200$ MPa

$h/R = 0.033$ and $\theta = 5^\circ$. The results are listed in Table 6 and plotted in Fig. 14a and b. Although the FCC packing and the HCP packing both refer to the same structure loaded in different directions, the elastic modulus, the yield stress and the plateau stress are all different, indicating the anisotropy property of the structure. The HCP packing gives the highest plateau stress (7% higher than that of the FCC packing), showing that it is the best one for energy absorption. The energy absorbing capacities of the BCC packing and the SC packing are not as good as those of the other two packing patterns because the formers have relatively looser structures. In fact, the stress–strain curve of the SC packing is more or less like that of a single sphere under uniaxial compression (refer to [12]).

4.4.4 Specific energy absorption

It is noted from Table 6 that the plateau stress of the HCP packing is 68% higher than that of the SC packing. Apparently, it is because more material included in the HCP representative block contributes to the energy absorption. To further evaluate the effects of the structural parameters on the energy absorbing capacities of the MHS material, we can define a Specific Energy Absorption (SEA) characteristic as

$$SEA = \frac{\int_{\varepsilon_Y}^{\varepsilon_D} \sigma^*(\varepsilon) d\varepsilon}{\rho_0 \cdot \rho_{RD}}, \tag{3}$$

where ρ_{RD} is the relative density of the packing pattern. Figure 15a shows the variation of SEA versus h/R for the FCC packing with $\theta = 5^\circ$, where almost a linear relationship is found. The variation of SEA for different packing patterns with $h/R = 0.033$ and $\theta = 5^\circ$ is presented in Fig. 15b, where apparently the SEA of the HCP packing manifest only 14% higher SEA than that of the SC packing. It is evident, therefore, that when the energy absorbed by a unit mass is considered, the relative sphere wall thickness must be a more important parameter than the packing pattern.

4.5 Strengths and limitations of the present studies

Different from the previous finite element studies conducted by Sanders et al. [3,4] and Gasser et al. [5–7], the present study has successfully simulated the total collapse behaviors of the hollow sphere structures with regular packing patterns. Adjusted by the relative density based on the open-celled foam theory, the predicted post-yield behaviors, especially the plateau stress, agree well with the experimental measurements. The proposed models have greatly simplified the geometry of the connections and make the simulations possible to be efficiently formulated by shell elements. The typical computation time is between 1 and 4 h in a personal computer of PIII 1 GHz and 1 G Ram. However, the

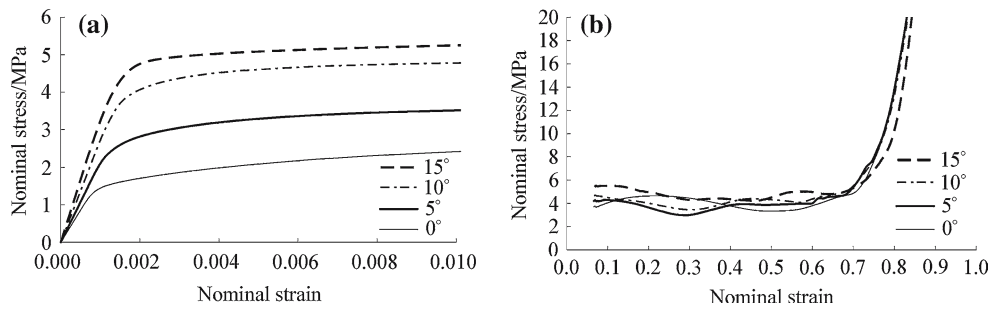


Fig. 11 Effect of the bonding angle; FCC packing with $h/R = 0.033$; $E = 200$ GPa and $Y = 200$ MPa: **a** Early response; **b** Large plastic response

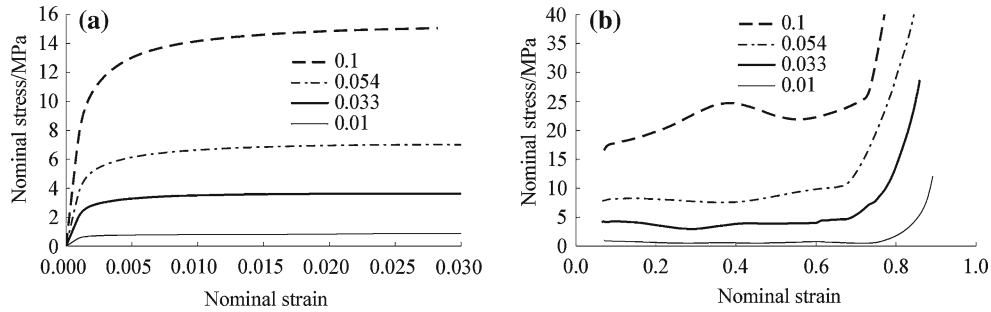


Fig. 12 Effect of the relative sphere wall thickness; FCC packing with $\theta = 5^\circ$; $E = 200$ GPa and $Y = 200$ MPa: **a** Early response; **b** Large plastic response

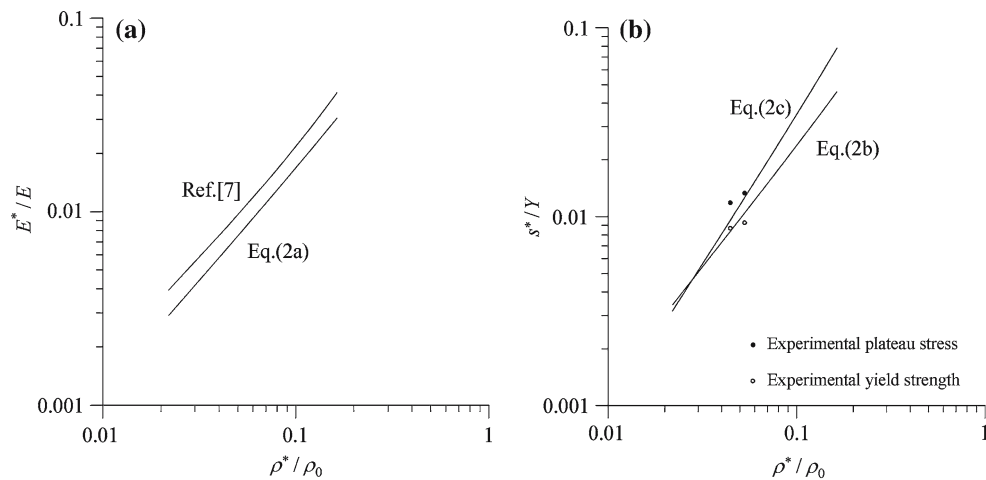


Fig. 13 **a** Elastic modulus for FCC packing; **b** Yield strength and plateau stress for FCC packing

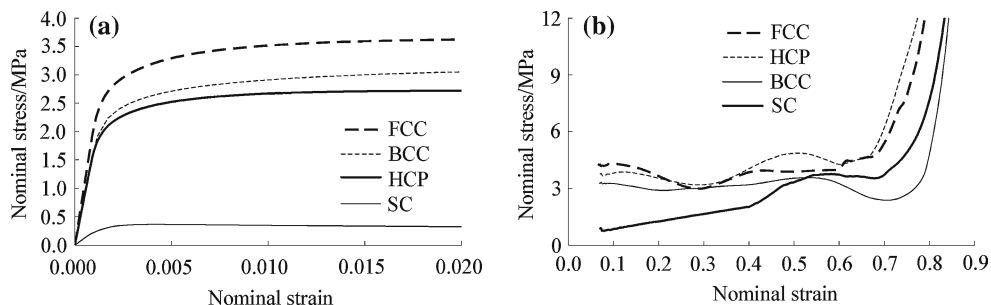


Fig. 14 Effect of the packing pattern; $h/R = 0.033$, $\theta = 5^\circ$; $E = 200$ GPa and $Y = 200$ MPa: **a** Early response; **b** Large plastic response

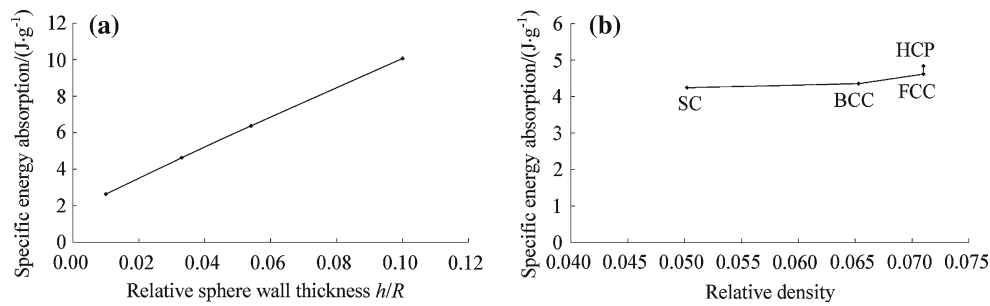


Fig. 15 **a** Variation of SEA versus h/R for the FCC packing with $\theta = 5^\circ$; **b** Variation of SEA for different packing patterns with $h/R = 0.033$ and $\theta = 5^\circ$

limitation also comes from the simplification of the connection, which is only valid for thin-walled spheres with small connect necks. Moreover, the symmetric boundary conditions should be replaced by the periodic ones so that the effect of the nominal Poisson's ratio can be evaluated.

5 Summary and concluding remarks

On the basis of the experimental observation of the MHS specimens under uniaxial compression, a simplified model is proposed to describe the connection between the neighboring spheres. It greatly reduces the geometric complexity of the structure, so that shell elements can be used to increase the computation efficiency.

By adopting the above idealization, finite element models of the SC packing, BCC packing, FCC packing and HCP packing are constructed, and their behaviors under uniaxial compression are successfully simulated with the commercial code ABAQUS v.6.4. The entire stress–strain curves are constructed by a combination of the static approach and the equivalent dynamic approach. The effects of all the governing input parameters are evaluated, whilst a special attention is paid to the plateau stress as it is directly related to the energy absorbing capacity of the material.

As for the geometrical parameters, a larger bonding angle results in a larger initial yield stress; and the plateau stress is in a power law relationship with the relative sphere wall thickness. The FCC packing and the HCP packing refer to the same structure loaded in different directions, but the predicted elastic modulus, initial yield stress and the plateau stress are all different, demonstrating the anisotropy property of the close-packed structure. Although the HCP packing is the best for energy absorption because of its highest plateau stress, the differences between various regular packaging configurations in the Specific Energy Absorption defined by Eq. (3) are in fact not significant (Fig. 15b), implying that

the relative wall thickness h/R plays a more important role than the packaging pattern (Fig. 15a).

Finally, the predicted plateau stresses agree well with the experimental data for both types of specimens. With the high efficiency of the computation, the finite element simulation is proven to be a powerful tool in evaluating the mechanical behavior of the MHS material in large deformations.

References

1. Waag, U., Stephani, G., Bretschneider, F., Venghaus, H.: Mechanical and acoustical properties of highly porous materials based on metal hollow spheres. In: Proceedings of the 2002 World Congress on Powder Metallurgy & Particulate Materials. Orlando, USA, Part 7 (2002)
2. Lim, T.J., Smith, B., McDowell, D.L.: Behavior of a random hollow sphere metal foam. *Acta Materialia* **50**, 2867–2879 (2002)
3. Sanders, W.S., Gibson, L.J.: Mechanics of hollow sphere foams. *Mat. Sci. Eng. A* **347**, 70–85 (2003)
4. Sanders, W.S., Gibson, L.J.: Mechanics of BCC and FCC hollow-sphere foams. *Mat. Sci. Eng. A* **352**, 150–161 (2003)
5. Gasser, S., Paun, F., Cayzele, A., Bréchet, Y.: Uniaxial tensile elastic properties of a regular stacking of brazed hollow spheres. *Scripta Materialia* **48**, 1617–1623 (2003)
6. Gasser, S., Paun, F., Riffard, L., Bréchet, Y.: Microplastic yield condition for a periodic stacking of hollow spheres. *Scripta Materialia* **50**, 401–405 (2004)
7. Gasser, S., Paun, F., Bréchet, Y.: Finite elements computation for the elastic properties of a regular stacking of hollow spheres. *Mat. Sci. Eng. A* **379**, 240–244 (2004)
8. Gao, Z.Y., Yu, T.X., Zhao, H.: Mechanical behavior of metallic hollow sphere (MHS) materials: an experimental study. *ASCE J. Aerospace* (2007, in press)
9. Zhao, H., Elnasri, I., Abdennadher, S.: An experimental study on the behavior under impact loading of metallic cellular materials. *Int. J. Mech. Sci.* **47**, 757–774 (2004)
10. Karagiozova, D., Yu, T.X., Gao, Z.Y.: Modeling of MHS cellular solid in large strains. *Int. J. Mech. Sci.* **48**, 1273–1286 (2006)
11. Stronge, W.J., Yu, T.X.: *Dynamic models for structural plasticity*. Springer, London (1993)
12. Ruan, H.H., Gao Z.Y., Yu, T.X.: Crushing of thin-walled spheres and sphere arrays. *Int. J. Mech. Sci.* **48**, 117–133 (2006)